Bulletin of the Seismological Society of America, Vol. 98, No. 3, pp. 1067–1084, June 2008, doi: 10.1785/0120070154

Seismic Cycles and Earthquake Predictability on East Pacific Rise Transform Faults

by Jeffrey J. McGuire

Abstract The concept of a seismic cycle, where the stress on a fault repeatedly builds up over a long period of time and then is rapidly released in a large earthquake, influences studies of both the basic physics of faulting and applied research aimed at estimating earthquake hazards. This hypothesis suggests that large earthquakes might be quasi periodic and that the probability of a particular portion of a fault rupturing twice in quick succession should be low. However, this basic hypothesis has been difficult to verify owing to the long repeat times of the largest earthquakes on most faults. East Pacific Rise (EPR) transform faults are an advantageous location to evaluate the seismic cycle hypothesis owing to their fast slip rates and the moderate size ($\sim M_w$ 6) of their largest earthquakes. Using surface-wave based determinations of the relative separations between earthquake centroids, I document 16 pairs of $M_w \geq 5.5$ events that had overlapping ruptures. The distribution of interevent times for these pairs is tightly clustered around 5 yr (with a coefficient of variation ~0.2) indicating that quasi periodicity may be prevalent for the largest events on these faults. Moreover, I find no pairs of overlapping M_w 5.5–6.2 earthquakes separated by less than 50 cm of elapsed plate motion, indicating that the two basic features of the seismic cycle hypothesis are evident in the timing of large EPR transform mainshocks. I have also confirmed earlier results demonstrating a high degree of short-term predictability of EPR mainshocks by combining teleseismic and hydroacoustic earthquake catalogs. Thus, there appears to be a high degree of both short and long-term predictability on EPR transforms.

Introduction

The fundamental concept of a seismic cycle was articulated following the 1906 San Andreas fault earthquake by Reid (1910), who hypothesized that earthquakes occur as the result of strain built up over a long period of time. Geodetic data has since confirmed that the far-field loading of plate boundary faults occurs as a slow steady build up of elastic strain. A simple view of this cycle of steady strain build up to a time-independent failure threshold followed by a nearly uniform stress drop in earthquakes suggests the hypothesis that at least the largest earthquakes on plate boundary faults should occur quasi periodically (Kanamori and Brodsky, 2004), and conversely that the probability of two large ruptures in quick succession on the same fault patch is low. However, if failure strength and stress drop vary strongly in time, then earthquake repeat times will be highly variable (Kanamori and Brodsky, 2004). Quasi periodicity is observed in numerical models of simple individual faults (Rice, 1993), and this assumption underlies many earthquake hazard estimates. If the seismic cycle concept is correct, there is at least some predictability in the earthquake system (Jordan, 2006). While the build up of strain is indeed slow and steady, the other necessary condition for quasi periodicity, that the failure threshold and drop in stress are spatially uniform and consistent from one large rupture to the next, is not well established, and considerable lines of evidence suggest that this view is at least somewhat incorrect.

Despite the geodetic evidence for steady-strain accumulation, it has been difficult to verify or reject the quasi-periodic nature of major plate boundary earthquakes because the instrumental records of large earthquakes only go back about 100 yr, while the seismic cycles for most plate boundary segments are likely in the range from 50–500 yr. The longest sequences of repeated large ruptures of the same plate boundary come from historical records in Japan and from paleoseismic records in various transform and subduction zone settings. Sykes and Menke (2006) recently reviewed the evidence for several historical and paleoseismic catalogs as well as the instrumental record at Parkfield, California, and found that many of these sequences were characterized by quasi-periodic behavior. They calculated maximum likelihood estimates of the coefficient of variation (CV) of the repeat times of the large plate boundary earth-

quakes. For perfectly periodic sequences, CV = 0, while for Poissonian behavior, CV = 1.0. Sykes and Menke found that most sequences had CV estimates smaller than 0.25, implying quasi-periodic behavior, essentially confirming the earlier results of Nishenko and Buland (1987). Thus, historical records indicate that large subduction zone ruptures are quasi periodic. However, examination of geodetic data from the Parkfield segment by Murray and Segall (2002) indicated that both the strictly defined time-predictable and slip-predictable models failed for this fault segment. Moreover, it appears that the Parkfield earthquakes do not always rupture the same asperity (Custodio and Archuleta, 2007) and have a somewhat higher CV (~0.37) than many subduction zones (Sykes and Menke, 2006). The combination of the observations on the accumulation (and lack of release) of slip deficit in Parkfield with the Sykes and Menke observations that many major faults are somewhat periodic suggests that the variability in the largest earthquakes is significant enough to cause simple definitions of quasi periodicity to fail.

Part of the difficulty in constraining the extent of quasi periodicity in subduction zone settings results from the difficulty in determining the size and rupture area of prehistoric earthquakes. There is considerable evidence from paleotsunami studies in both Cascadia (Nelson *et al.*, 2006) and Chile (Cisternas *et al.*, 2005) that individual portions of a subduction zone sometimes rupture in moderate (M 8) events in the intervals between the largest (M_w 9) events. Is a fault quasi periodic if M 9 ruptures happen every ~500 yr but M 8 ruptures are random? This basic issue of what earthquakes should be considered on a particular fault has caused some of the confusion in the evaluation of the quasi-periodic hypothesis. One way to quantify this choice is to characterize a particular fault system by its scaling relation for the number (or frequency) of earthquakes as a function of their seismic moment $N(M)$. The most common form for this distribution,

$$N(M) = N_0\left(\frac{M_0}{M}\right)\exp\left(\frac{M_0 - M}{M_c}\right), \qquad (1)$$

termed the modified Gutenberg–Richter distribution (Kagan and Jackson, 2000), includes a power-law scaling region that extends from small events to about the corner magnitude, M_c above which the frequency of events falls off rapidly due to the spatial extent of the fault. Discussions of periodicity are inherently about earthquakes with $M_w \geq M_c$ for a given fault, while smaller earthquakes (from the scaling region) appear to be controlled more by earthquake interactions than the long-term seismic cycle. As the paleoseismology of subduction zones clearly indicates, the size of the largest ruptures on a given plate boundary is somewhat variable, and this variability must be accounted for in evaluating the quasi-periodic hypothesis. Understanding the degree of variability superimposed on quasi-periodic behavior requires a dataset that covers many repeating patches and includes information on both the repeat times and the variation in seismic moment between events.

A closely related debate focuses on the seismic gap hypothesis, which states that major plate boundaries that have not had a great earthquake for a significant period of time are more likely to have one soon than those regions which have recently undergone a large rupture. The seismic gap hypothesis as formulated by McCann *et al.* (1979) presented one of the first physically motivated earthquake prediction experiments. The predictability of large earthquakes is usually discussed as long term (seismic cycle), intermediate term (few years), or short term (hours–days beforehand) with the seismic cycle concept supporting the highest level of optimism for long-term predictability (Sykes *et al.*, 1999). The intermediate-term forecast of McCann *et al.* was tested after ~10 yr by other authors and rejected in favor of a clustering hypothesis (Kagan and Jackson, 1991). However, there is considerable debate about the exact formulation of the hypothesis and whether it can be rejected (Jackson and Kagan, 1993; Nishenko and Sykes, 1993). Much of this confusion results from defining the following quantities: what is considered a large earthquake for a particular plate boundary, the spatial limits of a gap, how to measure whether a particular earthquake fills a gap or overlaps with a previous rupture, and the range of focal mechanisms relevant to a particular prediction. Clearly this hypothesis test would be more straightforward if it could be focused on a type of plate boundary for which the largest earthquake was well defined, that size earthquake occurred regularly in the instrumental record, and the focus was on whether candidate ruptures had substantial overlap in their moment-release zones rather than on the details of gap ends.

Midocean ridge transform faults (RTFs) have several advantages for studying earthquake predictability. Recent studies of global seismicity found that the largest earthquakes on RTFs (defined as M_c) depend on the thermal state of the fault with warm faults having smaller corner magnitudes (Bird *et al.*, 2002; Boettcher and Jordan, 2004). For short (50–150 km) transforms on the East Pacific Rise (EPR; Fig. 1), which typically slip at rates of 10–14 cm/yr, the corner magnitude estimates from Boettcher and Jordan's scaling relations are M_w 6.0–6.2 (95% confidence range) for a 120-km-long fault segment to M_w 5.8–6.0 for a 70-km-long fault segment. The ratio of the average slip in earthquakes of this size (50–100 cm) to the plate-motion rate suggests that the seismic cycle could be extremely short on EPR transforms (in the range of 5–10 yr). Moreover, McGuire *et al.* (2005), (hereafter MBJ) utilized earthquake locations from the National Oceanic and Atmospheric Administration's (NOAA's) hydroacoustic network (Fox *et al.*, 2001) to demonstrate that EPR transforms have a high degree of short-term predictability. Essentially foreshock sequences on these faults are about an order of magnitude more common than on faults in California. Owing to the foreshocks, even simple algorithms can achieve large probability gains over random guessing (McGuire *et al.*, 2005). Additionally,

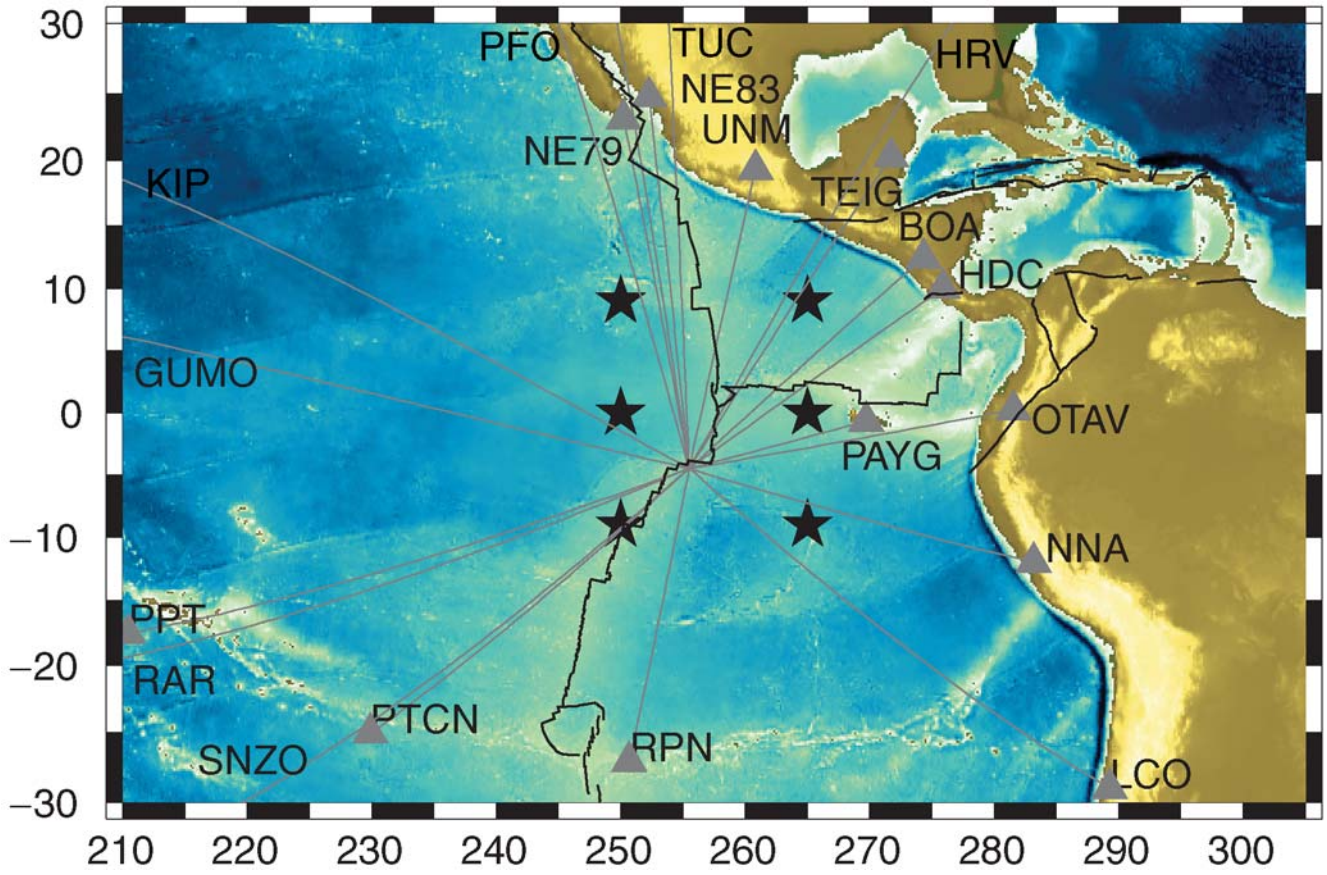

Figure 1. Location map of EPR transforms showing the NOAA hydroacoustic instruments (stars) and the GSN seismic stations (triangles and labels) and R1 ray paths used in this study.

the hydroacoustic earthquake catalogs demonstrate that deformation on EPR plate boundaries is localized to one fault strand (Figs. 2 and 3) and almost all the magnitude >3 seismicity is contained on the transform rather than spreading boundaries (Fox *et al.*, 2001).

In this study, I explore the extent of earthquake predictability on EPR transform faults in two ways. First, I extend the work of MBJ to determine if short-term predictability extends below the corner magnitude into the scaling region of the Gutenberg–Richter distribution. The MBJ study focused on 19 mainshocks in the Global Centroid Moment Tensort (CMT) catalog that overlapped the hydroacoustic catalog available at that time. Below I increase the set of available mainshocks by calculating moments for EPR transform earthquakes too small to be in the Global CMT catalog (available at www.globalcmt.org, last accessed March 2008) and by using a somewhat expanded version of the hydroacoustic catalog. Additionally, I study the long-term predictability of the same mainshocks by determining the time intervals between $M_w \geq 5.5$ earthquakes with significantly overlapping rupture areas. My results indicate that on these relatively simple, highly localized plate boundaries, there is considerable degree of earthquake predictability on both short and long terms.

Method

The accuracy and completeness level of global earthquake catalogs is insufficient for evaluating short and long-term predictability on EPR transforms. The Global CMT catalog is complete to approximately M_w 5.5, but it has location errors (~20–50 km) that are larger than the size of an individual EPR mainshock's rupture zone. The only available catalog with small location errors (~5 km) is the NOAA hydroacoustic catalog, which currently covers the time period from 19 May 1996 to 19 October 2002. While the NOAA catalog has highly accurate locations due to the slow propagation velocity of the *T*-phases it utilizes, it has poor magnitude information. The NOAA catalog provides a measure of earthquake size called the acoustic source level (ASL) (Fox *et al.*, 2001). While this quantity is correlated with earthquake size (see Results), there is considerable scatter owing to the limited dynamic range of the instruments, the high-frequency nature of the *T*-phase arrival, and the temporal variability in *T*-phase propagation efficiency. To improve the MBJ test of short-term earthquake predictability, accurate moment estimates are required for a larger number of EPR earthquakes that are currently in both the CMT and NOAA catalogs. To evaluate the long-term predictability on these faults, the relative location error of CMT catalog events must

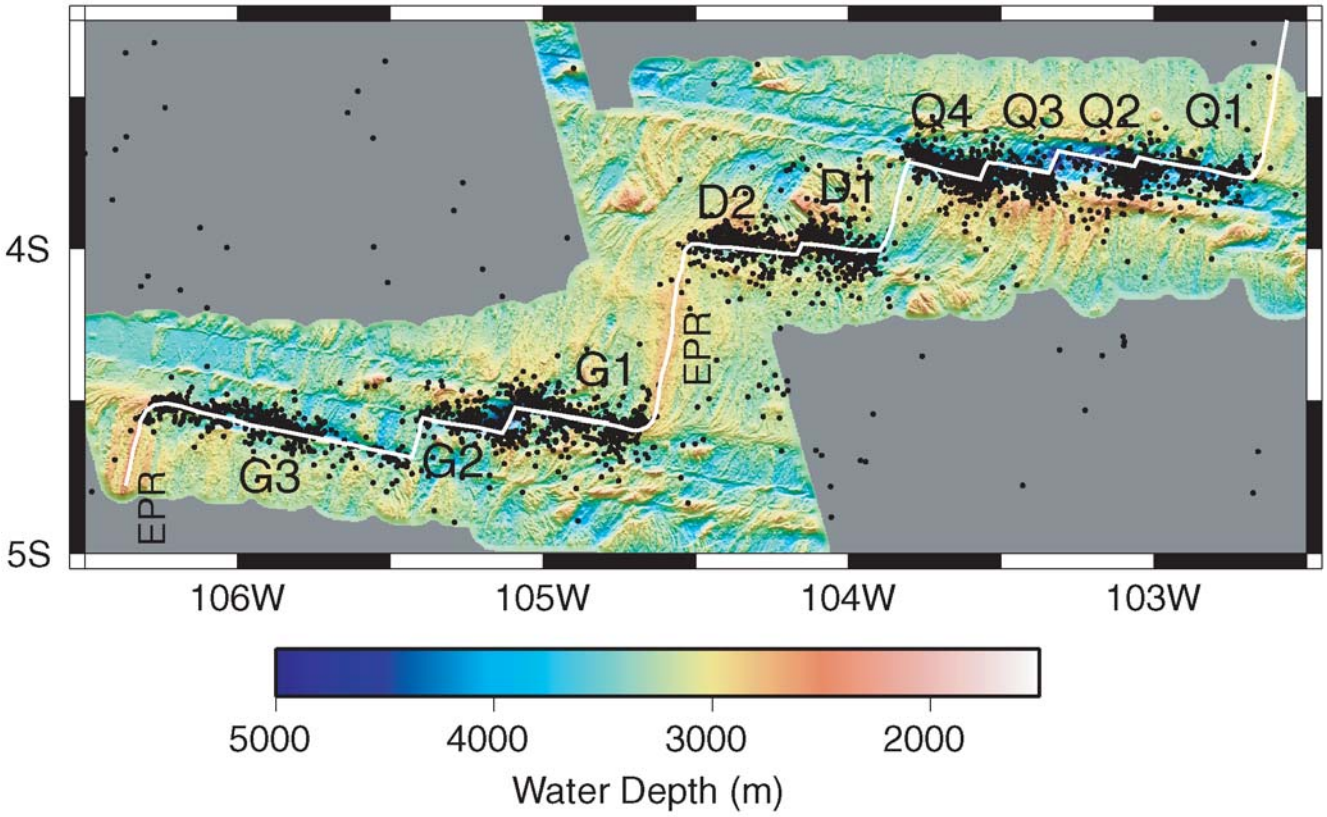

Figure 2. Location map of the Quebrada, Discovery, and Gofar transforms showing fault segments with the naming convention of Searle (1983). Bathymetry and plate boundaries (white lines) from Pickle and Forsyth (Forsyth *et al.*, 2006; Langmuir and Forsyth, 2007). Black dots denote the NOAA hydroacoustic earthquake locations.

be reduced enough to determine which pairs of events have overlapping rupture areas.

To constrain the moment and relative location of events, I use an approach based on measuring differential arrival times of first orbit Rayleigh waves by cross correlation. I utilize R1 waves in the frequency band from 0.02 to 0.04 Hz because of the high signal-to-noise ratio in this band and because the R1 group velocity is fairly constant in this band for young oceanic lithosphere (Nishimura and Forsyth, 1988), allowing arrival times to be interpreted in terms of source location differences rather than dispersion (Forsyth *et al.*, 2003). For EPR transform faults, the range of earthquake depths is expected to be contained to the oceanic crust (Trehu and Solomon, 1983). Additionally, all focal mechanisms are likely to correspond to a near-vertical strike-slip fault, as the NOAA catalog shows almost no seismicity associated with the spreading segments of the EPR. For each fault, I identified an event(s) in the Global CMT catalog that was recorded by an azimuthally distributed set of stations to use as an empirical Green's Function (EGF). Owing to the likely similarity in mechanism, depth, and location, the R1 arrivals at GSN stations from the hydroacoustically detected events are expected to have very similar waveform shapes to those from the EGF events, and the primary difference is expected to be in the amplitude of the arrival (i.e., the moment of the earthquakes). The assumption of identical moment tensors and centroid depths allows us to map this amplitude difference into an estimate of the seismic moment of the *T*-phase event. For every event in the NOAA catalog on the Quebrada, Discovery, Gofar, Yaquina, Wilkes, and Siqueiros transform

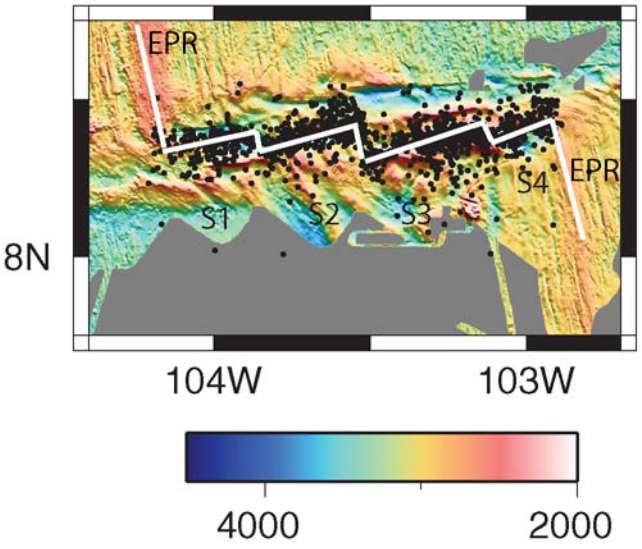

Figure 3. Location map of the Siqueiros transform fault showing fault segments S1–S4.

faults, I cross correlated the waveforms at global stations (Fig. 1) that correspond to the expected R1 arrival time with a similarly windowed recording of the EGF event's R1 arrival. Owing to the low-frequency band and small centroid separation distances, the cross-correlation coefficients typically exceed 0.95 for events with $M_w > 4.5$ (see Fig. 4). For each station, the relative moment of the *T*-phase event is calculated as the ratio of the peak of the cross correlagram to the EGF's autocorrelation at zero lag. The median of the individual station values is taken as the best estimate of the moment ratio between the EGF event and the *T*-phase event.

To estimate the relative position between two events, we utilize the differential arrival times measured from the peak of the cross-correlation functions (see Fig. 4). Differential times with a cross-correlation coefficient > 0.65 are fit to a cosine function using an L1 norm to minimize the effect of occasional outliers. The azimuth and direction of the *T*-phase event are calculated using the scale and phase parameters of the cosine along with the group velocity of the R1 waves in the source region (~3.7 km/sec). Standard errors for the cosine parameters are calculated using a bootstrap algorithm and assuming a Gaussian distribution with a 1-sec standard deviation for the differential travel-time measurement errors (Billings *et al.*, 1994; Shearer, 1997). For *T*-phase events, the event separation data is used to check that an appropriate EGF was chosen. Owing to occasional large mislocations in the *T*-phase catalog, the moment estimation/location process is sometimes requires a second iteration with a closer EGF. Additionally, the event separations are used in the evaluation of long-term predictability.

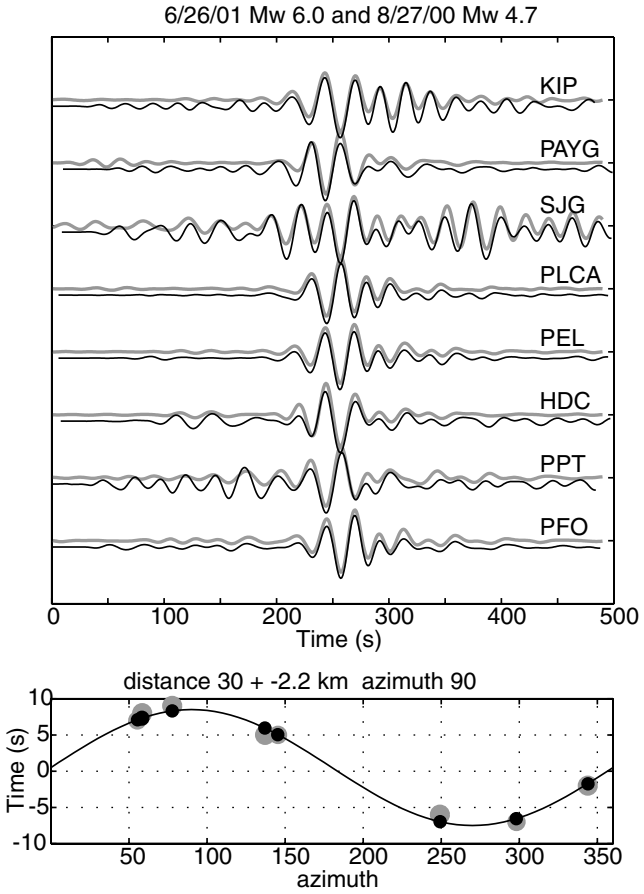

Figure 4. Example of the M_w estimation procedure for a *T*-phase event on 27 August 2000 on the Discovery transform. Seismograms from a Global CMT event (26 June 2001, shown in gray) are cross correlated with seismograms from the time of the *T*-phase event (shown in black). To determine the relative location differential arrival times (bottom panel, gray circles) are fitted using a grid search to minimize the L1 norm (black line and black dots). The moment ratio between the two events is estimated as the median of the values calculated at the individual stations from the peak of their cross-correlation function. In this case, the centroid of the *T*-phase event was located 30 km east and it had an M_w of 4.7.

Application of the surface-wave algorithm resulted in 326 M_w estimates ranging from 3.9 to 6.2 for earthquakes in the NOAA catalog. As previous studies have noted, there is an overall correlation between the ASL estimate of earthquake size and traditional seismic estimates of magnitude. However, even for earthquakes on a fault in the middle of the NOAA array, the scatter in the ASL estimates (Fig. 5) is large enough (about 1 unit in M_w) to prevent the ASL estimates from being reliable enough for detailed catalog analysis because may quantities (such as the expected number of aftershocks) depend exponentially on the earthquake magnitude. Additionally, our results imply that the detection threshold for the NOAA array is higher than previous estimates. Fox *et al.* (2001) concluded that an ASL of 210 corresponded to an m_b of 1.8. From Figure 5 it appears that an ASL of 210 would correspond to approximately M_w 3.5. Some of this difference results from the typical offset in m_b versus M_w for oceanic strike-slip earthquakes, but even after correcting for that effect (about 0.5–1 magnitude units), the detection threshold appears to be higher than the Fox *et al.* (2001) results.

Results

Short-Term Predictability

MBJ showed that foreshock sequences in the last hour before ($M_w \geq 5.5$) mainshocks are common enough on EPR faults to allow simplistic prediction algorithms to achieve significant probability gains over random guessing. The expanded catalog of M_w estimates contains enough $M_w \geq 5.0$ earthquakes to allow for a more detailed and robust evaluation of the short-term predictability on these faults. To formulate a well-posed prediction algorithm, I follow the retrospective algorithm of MBJ with two modifications. An alarm is issued following every hydroacoustically detected earthquake that an earthquake of a moment magnitude greater than or equal to m_p will occur sometime during time window of length t_p immediately following the hydroacoustic event and somewhere within a spatial window of radius r_p from the hydroacoustic location. We set $m_p = 5.0$ and because the deformation is localized to a single, nearly east–

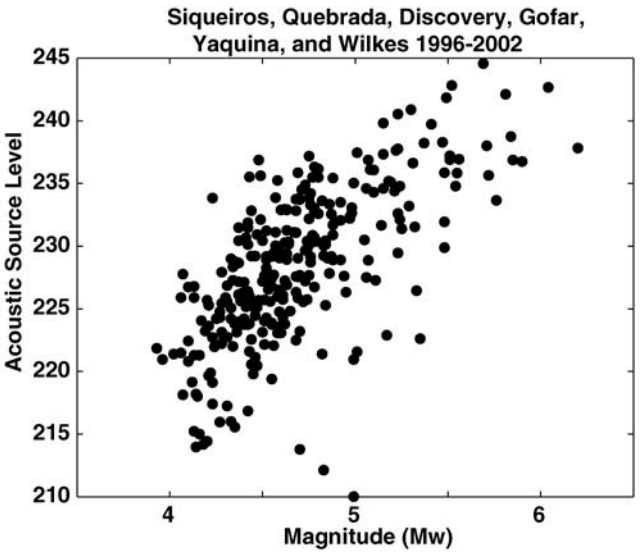

Figure 5. M_w estimates versus NOAA ASLs for 1996–2002 day 100 on the six EPR transform faults.

west fault strand at any particular location, we set the spatial window $(r_p) = \pm 15$ km of longitude. The first modification is that we issue alarms after every hydroacoustically detected earthquake instead of implementing a lower cutoff in ASL. The primary reason for this is the unreliability of the hydroacoustic estimates of source size (Fig. 5). Our second modification of the MBJ algorithm is to vary the time window, t_p, of the alarms from 10^3 to 10^7 sec. This allows the variation in the performance of the prediction algorithm as a function of the fraction of the space-time volume covered by alarms to be analyzed.

Alarm based prediction algorithms are often evaluated using Molchan's error diagram (Molchan, 1997), which compares the fraction of the space-time volume filled with alarms, τ, to the failure to predict rate, ν. By definition, all prediction algorithms include the $(\tau = 1,\ \nu = 0)$ and $(\tau = 0, \nu = 1)$ points, which correspond to filling the entire space-time volume and none of the space-time volume with alarms, respectively. To evaluate ν for a series of t_p values, a set of mainshocks to be predicted must be defined. To avoid the relatively easy task of predicting the aftershocks that follow large earthquakes, I apply a simple declustering algorithm to the catalog. A one week time period following every $M_w \geq 5.0$ earthquake is removed from consideration. This effectively removes the significant aftershock sequences from the catalog because of the unusually high difference in magnitude between RTF mainshocks and their largest aftershock (about 2.0 units [Boettcher and Jordan, 2004; McGuire *et al.*, 2005]) and the very fast temporal decay of aftershock sequences in the NOAA catalogs (Bohnenstiehl *et al.*, 2002). This leaves us with a dataset of 46 declustered mainshocks to be predicted on the six EPR faults (Table 1). To calculate τ for a particular value of t_p requires a numerical integration of the space-time volume because many of the alarms overlap (particularly for large values of t_p). To perform this integration the space-time volume is divided into cells that were 5 km by $t_p/3$ sec and counted the cell as filled by an alarm if any *T*-phase event occurred within t_p and r_p of the cells boundaries. Thus, I conservatively (slightly) overestimate the value of τ for a given value of t_p. The declustering procedure as well as the calculation of τ and ν for a given t_p were preformed separately for the four fault systems (QDG, Wilkes, Yaquina, and Siqueiros) and then combined based on the relative lengths of the four faults.

Table 1
The 46 Declustered EPR Mainshocks That Were Tested for Short-Term Predictability

Year	Month	Day	Hour	Minute	Second	M_w	Fault
1996	08	05	20	27	43	5.33	Y
1996	08	23	21	56	15	5.9	QDG
1997	02	26	00	21	00	5.21	W
1997	03	25	08	09	28	5.76	QDG
1997	04	07	17	53	07	5.72	QDG
1997	05	13	00	56	53	5.32	W
1997	06	08	21	02	43	5.06	QDG
1997	07	21	07	47	01	5.48	W
1997	08	07	13	42	29	5.1	S
1997	08	15	07	38	06	6.2	QDG
1997	11	02	01	02	35	5.07	QDG
1998	04	19	21	37	59	5.22	S
1998	05	10	06	35	50	5.51	S
1998	05	30	19	30	28	5.31	W
1998	07	25	09	54	01	5.23	W
1998	08	21	13	45	04	5.15	QDG
1998	08	25	18	44	31	5.23	W
1998	10	08	07	36	14	5.47	W
1998	10	16	01	54	12	5.48	QDG
1998	11	15	04	51	45	5.47	QDG
1999	02	26	11	38	03	5.17	W
1999	03	31	23	18	24	5.37	W
1999	05	18	06	15	08	5.15	W
1999	09	17	06	53	58	5.01	W
1999	09	18	04	01	22	5.51	QDG
1999	10	07	03	58	50	5.14	QDG
1999	11	10	02	25	57	5.55	Y
2000	01	04	17	42	49	5.23	QDG
2000	08	12	14	13	10	5.54	S
2000	10	20	19	47	21	5.48	QDG
2000	12	24	14	09	47	5.24	Y
2001	04	26	19	00	00	5.69	S
2001	05	31	10	19	25	5.18	W
2001	06	26	12	34	00	6.04	QDG
2001	07	23	09	43	08	5.29	QDG
2001	07	26	02	49	44	5.08	S
2001	09	17	16	43	44	5.49	W
2001	10	16	15	22	07	5.35	W
2001	11	29	17	07	10	5.52	QDG
2001	12	18	07	05	49	5.06	QDG
2002	01	24	21	07	54	5.81	QDG
2002	02	07	23	28	40	5.41	S
2002	06	17	13	13	15	5.37	QDG
2002	09	03	22	10	02	5.03	W
2002	09	18	04	29	06	5.22	W
2002	10	05	05	52	43	5.07	S

The summary error diagram for the EPR transform faults shown in Figure 6 demonstrates that short-term predictability

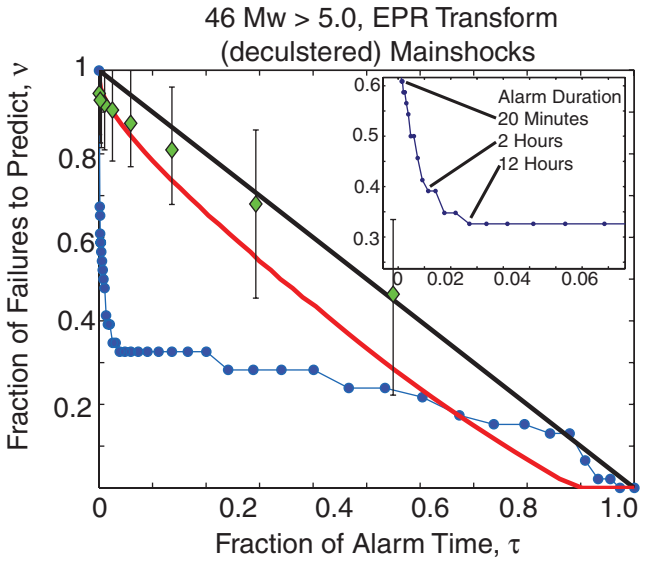

Figure 6. The error diagram (Molchan, 1997) for 15-km radius prediction windows for all M_w 5.0 earthquakes on the Quebrada, Discovery, Gofar, Wilkes, Yaquina, and Siqueiros transforms. The mainshock catalog contains 46 events between 1996 and 2002 that were not preceded in the previous week by an M_w 5.0 event on the same fault system. Blue dots indicate the success rates for logorithmically spaced alarm durations ranging from 1000 sec (upper left) to a year (lower right) after every hydroacoustically detected event. The black line denotes the expected value for unskilled predictions (i.e., random guessing) and the red curve the 99% confidence bound for such predictions. The green diamonds show the results of applying the same declustering and prediction algorithms to a suite of 100 synthetic earthquake catalogs generated by the ETAS seismicity model The diamonds are plotted at the median values of v, and the error bars denote the 95% confidence region for the results from applying the algorithms to the ETAS catalogs. The inset shows the interesting region for our short-term predictions. Most of the curvature in the blue curve corresponds to predictions ranging from about 30 min to 12 hr in duration (inset).

is a robust conclusion. The prediction algorithm was evaluated for 40 logarithmically spaced values of t_p ranging from 10^3 to 10^7 sec. The topology of the error diagram curve in Figure 6 is unusual in that it shows a fairly sharp transition between a steep slope at low values of τ to a low slope at moderate and high values of τ. For studies using synthetic catalogs produced by various clustering models (Newman and Turcotte, 2002; Helmstetter and Sornette, 2003; Kagan, 2007), error diagrams are typically smooth concave up curves. For studies using real earthquake and volcanic eruption datasets, there are usually not enough mainshocks to sample the error diagram curve densely (Kellis-Borok *et al.*, 2002; Grasso and Zaliapin, 2004) but these curves appear to have relatively smooth variations similar to the synthetic studies. In contrast, the EPR error diagram clearly has two regimes separated at about $t_p \approx 10$ hr.

The presence of two regimes in the error diagram may suggest the presence of two underlying processes. Kagan (2007) produced a similar error diagram using a synthetic catalog comprised of two Poisson renewal processes with different scale parameters. Essentially, after each earthquake, the PDF for the time of the next earthquake was chosen to be from either process 1 or process 2 with probabilities p_1 and p_2 (where the timescale of process 1 is less than that of process 2). The value of ν at the kink in the error diagram curve equals the fraction of events triggered by process 2, and the value of τ at the kink in the error diagram corresponds to the ratio of the two timescale parameters. I reproduced Kagan's result in Figure 7 with parameter values that mimic the behavior of the EPR catalog, namely a ratio of timescales ~500 and about 60% of earthquakes triggered by the short timescale process. The similarity between Figures 6 and 7 suggests that there may be two different triggering processes of roughly equal strength that control the timing of the set of declustered EPR mainshocks.

One shortcoming of evaluating earthquake prediction algorithms with the error diagram is that random guessing (e.g., the diagonal line in Fig. 6) is a very easy null hypothesis to reject. To provide a more conclusive demonstration that the short-term predictability of EPR earthquakes is not simply a result of general earthquake clustering behavior, we calculated 100 synthetic earthquake catalogs using the space-time epidemic-type aftershock sequence (ETAS) methodology (Helmstetter and Sornette, 2002, 2003). The catalogs were all generated with an identical set of ETAS parameters ($p = 1.2$, $\alpha = 0.8$, branching ratio $= 0.1$, $\mu = 3$, M_0 1.0, M_d 3.0, M_{max} 6.5) that are equal to the average values for EPR transforms determined in the MBJ study (e.g., for branching ratio, p, and α). The background seismicity rate was chosen so that a comparable number of mainshocks would exist in the synthetic and real EPR catalogs. We then applied the declustering and prediction algorithms discussed previously to the synthetic catalogs. The only difference is

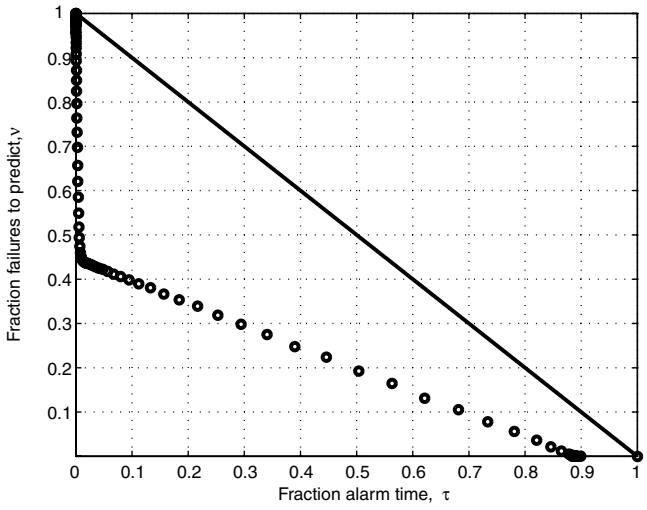

Figure 7. After Kagan (2007). Error diagram for a synthetic earthquake catalog generated using a mixture of two renewal processes. This is identical to the example in figure 5 of Kagan (2007) except for our choice of the fraction of the catalog generated with the short timescale process (55%) and the ratio of the scale parameters (500).

that the ETAS catalogs cover two spatial dimensions instead of effective one (e.g., fault length) for the real EPR catalog. To account for this, the spatial window of the prediction algorithm was fixed at a radius of 20 km such that an individual prediction covers the same fraction of the total spatial window in both the real and synthetic cases. The green diamonds in Figure 6 show the median values of ν for a series of window lengths, and the associated error bars denote the range that contained 95% of the ETAS simulations. The behavior of the prediction algorithm on the ETAS sequences is relatively straightforward in that, at short time windows, it captures the fraction of the catalog that is triggered by other earthquakes (e.g., branching ratio of $0.1 \sim \nu = 0.9$) while at longer windows, the performance of the algorithm mirrors that of random guessing because the mainshocks triggered by background loading in ETAS are expected to be randomly distributed in time. The observation in Figure 6 that our simple prediction algorithm works so much better for EPR seismicity than for synthetic ETAS seismicity demonstrates that there is a significant level of short-term earthquake clustering immediately before large earthquakes on the EPR that results from a physical mechanism that is not accounted for by the ETAS scaling relations.

Long-Term Predictability and Seismic Cycles

I estimated the separation between the centroids of pairs of $M_w \geq 5.5$ earthquakes on the Gofar, Discovery, Quebrada, and Siqueiros faults to determine if large earthquakes on these faults rupture quasi periodically. While no two large earthquakes are identical, a logical criterion for defining repeating mainshocks is that their rupture areas had considerable overlap. The rupture areas of $5.5 \leq M_w \leq 6.2$ EPR earthquakes cannot be determined directly from the available data. So I use a simple rule based on similar sized continental earthquakes. If the two centroids are separated by less than half of their expected rupture length, then the pair is designated as overlapping. In particular, if at least one event in the pair has an $M_w \geq 6.0$, then I use $L/2 = 10$ km, but if both are smaller than M_w 6.0, then I use $L/2 = 5$ km as our criteria to define significant overlap. Given the rupture length estimates for well recorded onland events in this size range (e.g., 2004 Parkfield, M_w 6.0 has $L \sim 20$–25 km; Johanson *et al.*, 2006), the criteria are conservative. Additionally, Figure 8 demonstrates that the one-day aftershock areas for M_w 6 EPR mainshocks extend 30–50 km along strike. While the aftershock areas are likely larger than the true rupture area, they are the best direct estimate available of EPR rupture lengths. Owing to the relatively thin (~4 km) seismogenic zone expected for EPR transforms (Trehu and Solomon, 1983), EPR mainshocks may have longer ruptures than continental strike-slip earthquakes with the same moment. In addition to Figure 8, there is some evidence of unusually long ruptures for oceanic transform quakes from *T*-phase aftershock locations on the Blanco transform fault (Dziak *et al.*, 2000). Thus, our criteria for determining overlap (centroids within 5–10 km) are likely to be conservative compared to true rupture areas.

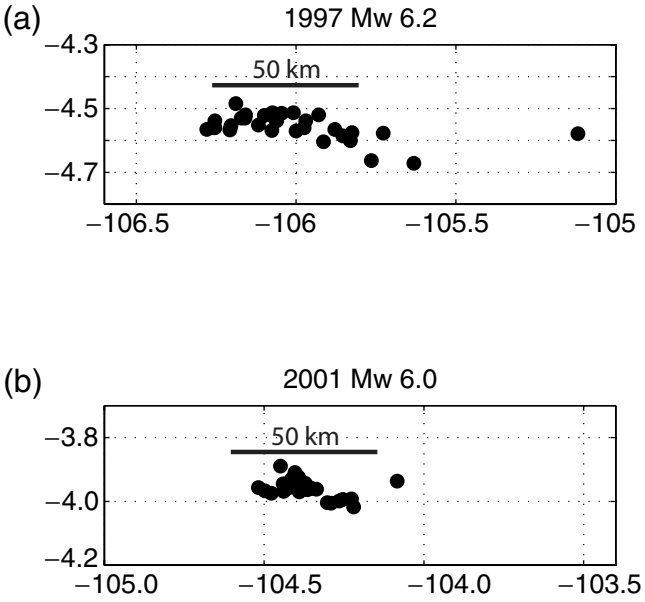

Figure 8. (a) One-day aftershock locations from the NOAA hydroacoustic catalog for an M_w 6.2 earthquake on the Gofar transform that occurred on 15 August 1997. (b) An M_w 6.0 earthquake on the Discovery transform that occurred on 26 June 2001. Formal location errors are <5 km for these faults according to the NOAA catalog.

I searched all possible combinations of $M_w \geq 5.5$ earthquakes for the Gofar, Discovery, Quebrada, and Siqueiros faults for the period from 1995 until January 2007 for overlapping ruptures. For events before 1995, it is often difficult to get a well-constrained estimate of the centroid separation for a pair of events due to the limited availability of seismic stations in the eastern Pacific. I obtained solid constraints on the relative locations of one event from 1992 (on the Gofar transform) and one from 1993 (on the Siqueiros transform). For other CMT catalog events in the 1990–1994 time period, I was not able to definitively determine if they overlapped with a subsequent rupture or not. In total, I found 16 pairs of overlapping ruptures, which are listed in Table 2. Figures showing the stations utilized, waveforms, and differential arrival times for each of these pairs are in the Appendix. One pair of events listed in Table 2 has a centroid separation of 14 km, but it is still included in the list of overlapping ruptures because the 2002 day 168 (13:26:05.00) event is a doublet with an unusually long rupture length. While this earthquake is listed in the CMT catalog as a single event, an analysis of its surface-wave directivity by Llenos and Forsyth (2007) demonstrated that it was comprised of at least two large subevents separated by ~30 km. For this pair (#7), the relative centroid locations were measured at very-low frequencies ($<$ 10 mHz) to ensure that the cross-correlation peak was sensitive to the whole 2002 rupture. Combining the results of Llenos and Forsyth with our centroid separation indicates that the 1997 event occurred within 5–10 km of the western 2002 subevent. The other unusual event in our

Table 2

Our Estimates of the Separation Distances for the 16 Pairs of EPR Mainshocks with Overlapping Ruptures

Number	Fault	Year	Day	Time (hh:mm:ss)	M_w	Year	Day	Time (hh:mm:ss)	M_w	Δx (km)	M_0 Ratio	Δt (yr)
1	G3E	2002	168	13:26:05	6.0	2007	216	14:25:01	6.0	3.7 ± 4.4	1.1	5.1
2	D2E	2001	333	17:07:06	5.5	2007	204	06:03:55	5.6	0 ± 3.5	1.3	5.6
3	D2	1998	319	04:51:49	5.5	2007	204	06:00:38	5.5	1.9 ± 3.1	1.0	8.7
4	G2	2002	168	13:18:06	5.8	2007	015	21:19:42	5.6	2.8 ± 2.2	1.7	4.6
5	G1	2002	024	02:07:18	5.8	2006	323	18:57:38	6.0	3.7 ± 2.3	2.3	4.8
6	S	2001	116	18:59:56	5.7	2006	284	06:00:50	5.8	0.0 ± 4.1	1.1	5.5
7	G1	1999	261	04:01:11	5.6	2006	323	18:57:38	6.0	7.4 ± 2.2	5.2	7.2
8	S	1998	131	01:34:40	5.8	2004	317	20:13:17	5.6	3.7 ± 6.5	2.0	6.5
9	G3W	1997	227	07:37:55	6.2	2003	249	02:08:19	6.0	3.7 ± 3.1	1.8	6.1
10	G3E	1997	084	08:09:25	5.7	2002	168	13:26:05	6.0	14 ± 2.8	3.6	5.2
11	D2E	1996	236	22:19:04	5.8	2001	333	17:07:06	5.5	0 ± 4.1	3.7	5.3
12	D2W	1996	236	21:56:13	5.9	2001	177	12:34:00	6.0	0 ± 3.3	1.4	4.8
13	G1W	1995	364	03:26:17	6.1	2003	164	18:24:09	5.7	9.2 ± 2.3	3.8	7.5
14	D1	1995	259	22:49:22	5.6	2001	211	04:34:50	5.6	2.8 ± 3.4	1.1	5.9
15	S	1993	186	06:54:15	5.6	1998	131	01:34:40	5.8	3.7 ± 3.1	2.2	4.8
16	G3W	1992	198	06:35:43	5.8	1997	227	07:37:55	6.2	1.9 ± 4.9	3.7	5.1

The moment ratio is defined as the larger event divided by the smaller event, regardless of which occurred first.

dataset is the 2006 day 323 (18:57:38), M_w 6.0 earthquake, which overlapped with two smaller events, an M_w 5.8 in 2002 and an M_w 5.6 in 1999. The 2002 and 1999 ruptures had a centroid separation greater than 5 km, so I do not classify them as overlapping ruptures. Instead, this appears to be a case of a fault patch breaking in two sections in one cycle and only one (larger) rupture in the next cycle. A scenario that is common in subduction zones.

For the quasi-periodic hypothesis to be even somewhat valid, the repeating ruptures should have fairly similar seismic moments and the interevent times should have a fairly peaked distribution centered on the ratio of the average mainshock slip to the faults geologic slip-rate. Figures 9 and 10 show histograms of these quantities, moment ratio, and interevent time for the overlapping pairs in Table 2. There are no direct constraints on the average mainshock slip (i.e., stress drop) for the EPR mainshocks, but if they are similar to continental earthquakes of the same moment, their average slip should be ~50 cm to 1 m. The plate-motion rate for the EPR transforms is approximately 14 cm/yr, indicating that recurrence times of 4–7 yr might be expected. Indeed the distribution of interevent times is contained to this region with a peak at ~5 yr. There is no clear trend of interevent time scaling with either the moment of the first or second event of the pair (Table 2). Figure 10 demonstrates the extent of variability in seismic moment between paired events. This quantity is not typically available in studies of the quasi-periodic hypothesis that involve geologic and/or historical estimates of earthquake size. Our results indicate that ratios of the seismic moments ranging from 1 to 5 are common.

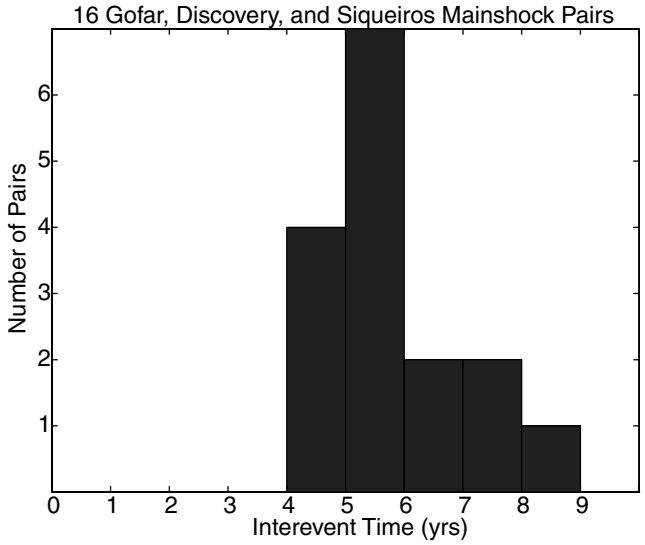

Figure 9. Recurrence intervals for the 16 overlapping mainshock pairs in Table 1.

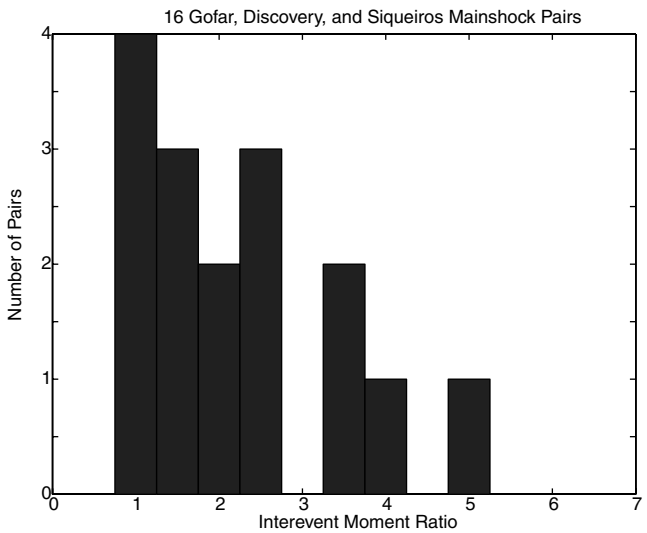

Figure 10. Moment ratios for the 16 mainshock pairs in Table 1.

Additionally, no strong correlation between the moment ratio and the interevent interval is observed.

Figure 9 and Table 1 demonstrate that I find no pairs of overlapping events separated by less than 4 yr (> 50 cm of plate motion). This is an interesting result both because of the nature of EPR seismicity and the corollary to the quasi-periodic hypothesis that immediately after a large earthquake, the same portion of the fault is not expected to fail again soon. This corollary is essentially the opposite of seismic hazard estimates that assign a Poisson distribution to individual faults. The EPR transforms are an interesting location to investigate the Poisson hypothesis because they are notable for having numerous pairs of similar sized mainshocks separated by a few hours (McGuire *et al.*, 2005). In all cases where two $M_w \geq 5.5$ earthquakes happened within a few days of each other, the event separations were larger than 10 km, indicating that the rupture areas likely did not overlap.

To further demonstrate the inadequateness of recurrence interval distributions that include significant probability of short intervals (e.g., less than half the median), we calculated a synthetic recurrence distribution by randomizing the origin times of the 24 $M \geq 5.5$ earthquakes on the QDG fault system between 1 January 1995 and 23 October 2007 (e.g., a random time was chosen for each event from a uniform distribution between these dates). We then calculated recurrence intervals for the 12 mainshock pairs in Table 2 that fall into this time-space window. For the asperities that have undergone multiple repeats in the 1995–2007 time frame, we only considered repeat times for nearest neighbors in time to mimic the analysis in Table 2. This procedure was repeated 30 times to generate a smooth cumulative fraction versus recurrence interval curve (dashed line in Fig. 11). This synthetic/hypothesized distribution was tested against the observed recurrence interval distribution using a Kolmogorov–Smirnoff (KS) test. The hypothesized (random) distribution of repeat times can be rejected at the 99% confidence level based on the KS test (Fig. 11). A similar observations that some sort of renewal model is favored over Poisson-like distributions has been made for a number of paleoseismic datasets (Nishenko and Buland, 1987; Ogata, 1999; Sykes and Menke, 2006).

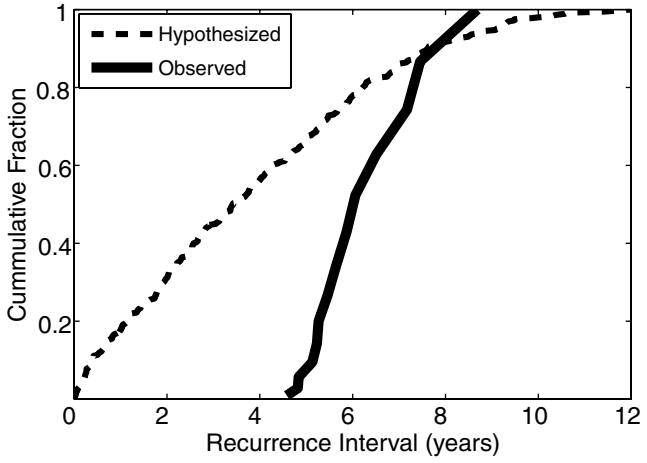

Figure 11. Results of a Kolmogorov–Smirnoff test comparing the observed distribution of repeat times for $M_w \geq 5.5$ event pairs (solid curve) and a hypothesized distribution (dotted line) calculated by randomizing the times of the large earthquakes in our catalog (see text). The hypothesized (randomized) distribution can be rejected at the 99% confidence level primarily due to the lack of earthquake pairs with short recurrence intervals.

Discussion

The relatively narrow histograms for the time interval between overlapping ruptures as well as for the moment ratio between these events indicates a robust seismic cycle. This difference relative to studies of subduction zones may simply result from our restriction of the event size to those with $M \geq M_c$. For instance, for the 1960 Chile rupture area, it is likely that many of the ($M_w \sim 8.5$) events that call quasi periodicity into question are actually a factor of 30–50 smaller in seismic moment that the 1960 (M_w 9.5) event. A similar moment ratio on the EPR faults corresponds to looking for overlap between M_w 4.5–5.0 events to larger M_w 5.5–6.0 ones. Thus our study of quasi periodicity is limited to a smaller range of mainshock magnitudes than some previous ones.

Figures 12 and 13 present space-time plots of the seismicity in the 1990–2007 time frame for the Quebrada, Discovery, Gofar system (Fig. 12) and the Siqueiros transform faults (Fig. 13) to portray the extent to which a Reid style seismic cycle may control the timing of the largest earthquakes on EPR transforms. The earthquake times and locations are color coded by magnitude so that the largest ($M_w \geq 5.5$) are easily identified (large red circles). The 16 pairs of events listed in Table 1 have been connected by black lines in Figures 12 and 13. The Discovery and Gofar faults (104 to 106.2 W in Fig. 12) have the strongest evidence for a seismic cycle with clusters of $M_w \geq 5.5$ events in 1992–1993, 1996–1997, 2002–2003, and 2006–2007. These time periods have been highlighted by the gray boxes in Figure 12 and appear to indicate a general (though not monotonic) westward migration of seismicity within each cycle. The lack of a clear connection between the events in the 1992–1993 cycle and the 1996–1997 cycle in Figure 12 is due to the limited availability of eastern Pacific seismic stations for the 1992–1993 cycle. Relative locations of these events are unreliable due to large azimuth gaps. It is also interesting to note that the $4.5 \leq M_w < 5.5$ seismicity (small yellow circles) appears to be relatively uniformly distributed in time. The Siqueiros fault has less large earthquakes and fewer pairs so while the interevent times are similar to the QDG system, the seismic cycle is not as clear in Figure 13.

The synchronization of the various repeating ruptures in Figure 12 is surprising. While static/dynamic triggering may explain some of the synchronization, several of the segments are separated by large ridge segments (10–50 km) and sig-

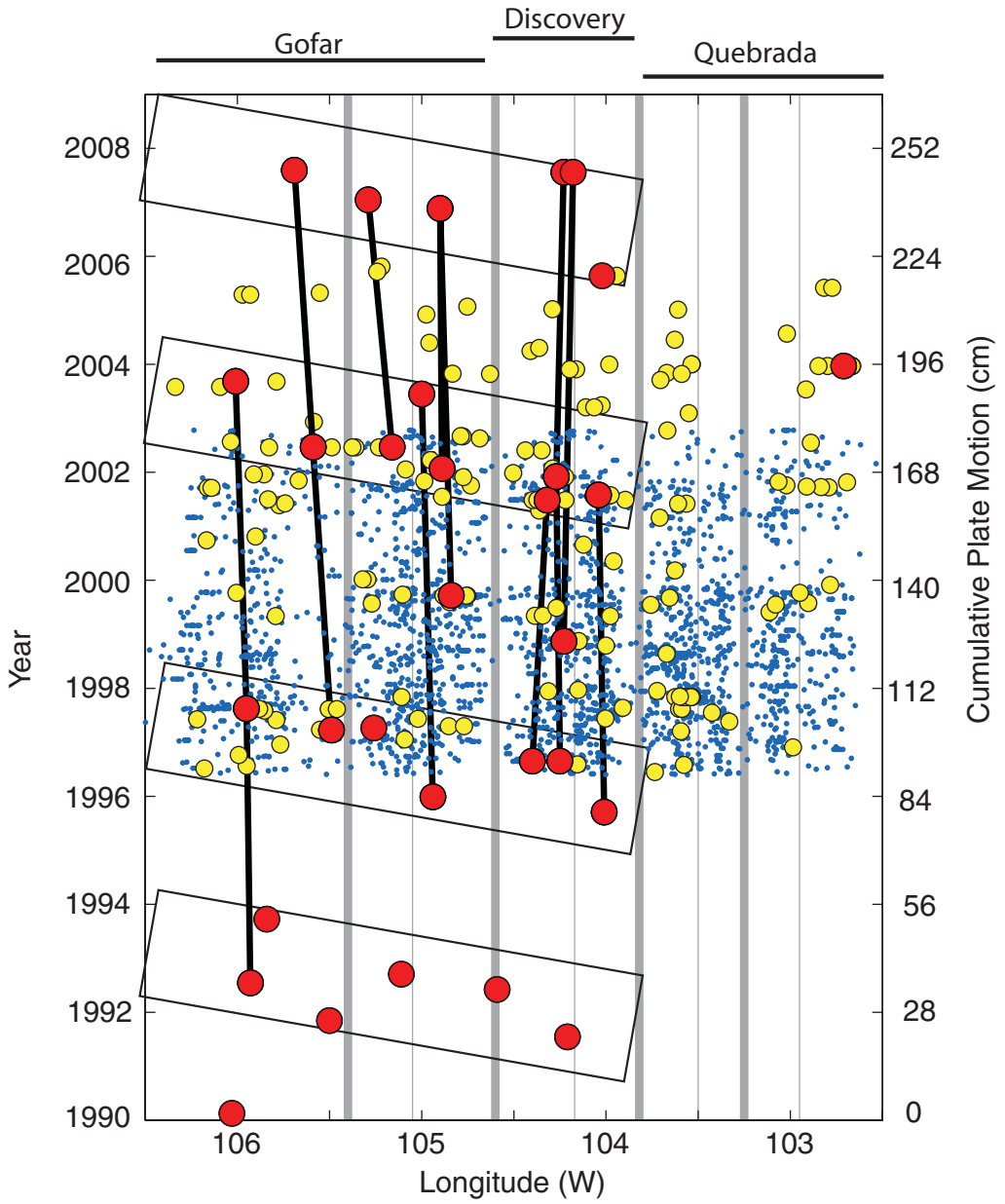

Figure 12. Representation of the combined NOAA, Global CMT, and our earthquake catalogs for the Quebrada, Discovery, and Gofar transform faults for the time period from 1990–2007. Every hydroacoustic detection is shown at its NOAA longitude estimate with a blue dot, unless it has an M_w estimate $\geq$4.5, in which case it is shown as a yellow circle. Additionally, earthquakes in the Global CMT catalog with an $M_w \geq 5.5$ are shown at their Global estimated longitude (large red circles). Pairs of $M_w \geq 5.5$ mainshocks that have been determined to have overlapping rupture areas are connected by black lines, which are not vertical due to errors in the CMT estimates. Major and minor spreading centers are shown by thick and thin gray lines, respectively. Cumulative expected plate motion (i.e., far-field fault loading) since 1990 is shown on the right-hand *y* axis. The gray boxes (each 2 yr wide) have been rotated and aligned with the time periods of high activity for $M_w \geq 5.5$ mainshocks. Twenty-seven of the 31 $M_w \geq 5.5$ earthquakes fall into the gray boxes that appear to denote the end of the seismic cycle on the Discovery and Gofar faults.

nificant delay times (weeks–months) that would rule out simple models of static and dynamic triggering. Lynch *et al.* (2003) investigated the conditions under which two fault segments separated by a creeping section would have seismic cycles that were synchronized in time as well as a single-peaked recurrence interval distribution. They found that small creeping sections and low mantle viscosities favor synchronization by allowing postseismic relaxation to communication between segments. Moreover, for the segments to have similar recurrence times, the peak strength and stress drop had to be roughly equal between the two segments regardless of other parameters. Thus, the minimal variation in

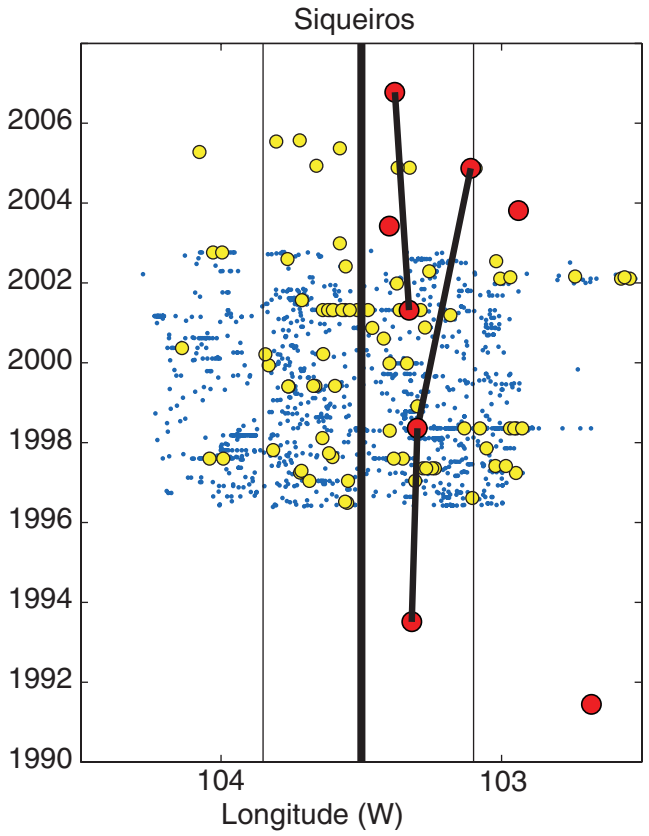

Figure 13. Plot of the combined earthquake catalog for the Siqueiros fault. Symbols are the same as in Figure 12.

recurrence interval can likely be used as a constraint on models that predict variations in transform fault rheology due to variations in plate tectonic parameters (Behn *et al.*, 2007).

The Quebrada fault (~102.5–104 W in Fig. 11) generated far fewer $M_w \geq 5.5$ mainshocks during the 1990–2007 time period than the Gofar and Discovery faults despite slipping at the same rate and having fault segments of similar length (Searle, 1983). The Quebrada fault had only one $M_w \geq 5.5$ earthquake during the entire 17-yr period (~240 cm of plate motion). This appears to be a creeping fault with very little seismic moment release. Boettcher and Jordan (2004) concluded that while ~75% of plate motion occurs aseismically on oceanic transforms, particular patches of OTFs must sometimes slip seismically and other times aseismically to explain various seismicity scaling relations. They termed this behavior the multimode hypothesis. The 2003 M_w 5.7 event on the Quebrada transform may be an example of multimode behavior. Assuming it had a similar stress drop to other QDG mainshocks, it would be expected to have at least one overlapping rupture of similar size during the 17-yr period unless the patch which ruptured seismically in 2005 sometimes also slips aseismically. The M_w 5.7 event occurred at the end of a day long swarm of strike-slip earthquakes, indicating that this generally aseismic fault may produce its largest earthquakes when transient stressing phenomena (creep, magma intrusion, or fluid flow) are occurring. The swarms may indicate a significant increase in stress or strain rate (Lohman and McGuire, 2007) that allows a larger region of the fault to rupture seismically.

Figure 12 suggests that a Reid style seismic cycle may control the long-term timing of large EPR transform earthquakes, but perhaps more surprisingly, Figure 6 indicates that there is likely a short-term triggering process that controls the timing of many mainshocks on a timescale of a few hours. The defining property of EPR transform seismicity as revealed by the NOAA catalog (McGuire *et al.*, 2005) and OBS deployments (Forsyth *et al.*, 2003) is that many of the largest earthquakes happen during earthquake swarms that last from a few hours to a few days (Roland *et al.*, 2004). These swarms account for the steep slope of the error diagram curve for values of $t_p < 10$ hr. Earthquake swarms are common on the strike-slip plate boundary faults running all the way from the EPR up the Gulf of California and into the Salton trough. A recent Salton Trough swarm was documented to be associated with a large shallow creep transient that likely drove the swarm (Lohman and McGuire, 2007). Given the large fraction of aseismic slip occurring on RTFs (Bird *et al.*, 2002), it is likely that the EPR swarms result from the same process as the Salton Trough swarms. This suggests a view of EPR faults where a Reid style cycle slowly raises the stress near the failure threshold (controlling the long-term predictability), while a transient event such as fault creep or fluid flow triggers the swarms of moderate and large earthquakes and controls the short-term predictability.

There are a number of $M_w \geq 5.5$ events that do not have an overlapping rupture during the time period when the global network should have been able to detect such events. This is likely an artifact of the combination of the factor of 2–6 variability in moment between repeaters and our arbitrary cutoff at M_w 5.5. The missing events may simply be M_w 5.4. There are no $M_w \geq 6.0$ events on the QDG system that have a missing repeater. Given the error bars in our estimates of relative centroid locations (a few km) and the lack of local networks, a longer dataset of $M_w \geq 6.0$ earthquakes will be required before we can determine if a fault patch can go more than ~7 yr after rupturing in an $M_w \geq 6.0$ without being followed by a repeat.

Determining whether a simple isolated fault is better described by a seismic cycle model or a more chaotic clustering model is a fundamental building bloc of time-dependent seismic hazard studies. This is a difficult question to answer in regions like California where multiple sub parallel faults accommodate plate-motion; these faults interact regularly, and the time between large ruptures is hundreds or thousands of years. However, both analysis of historic/geologic datasets (Ellsworth *et al.*, 1999) and large-scale computer models of interacting fault networks (Yakovlev *et al.*, 2006) have suggested CV values around 0.5. In contrast, both the Sykes and Menke (2006) and Nishenko and Buland (1987) studies of primarily historical subduction zone ruptures as well as our study of oceanic transforms find CV estimates around

0.2. This may simply reflect the tectonic setting where the major plate boundary faults in subduction zones and oceanic transform faults are relatively isolated from other major fault zones and hence see less variability in their recurrence intervals. At a minimum, the difference between these studies indicates the need to develop as many instrumental catalogs with multiple repeat ruptures as possible given geologic slip rates. While the EPR seismicity catalog is just beginning to have a sufficiently long instrumental record to address this question directly, it appears to support the general view that the ruptures with $M \geq M_c$ are quasi periodic. However, even the initial results presented here indicate that the seismic moment can vary by at least a factor of 5 between repeated large ruptures of the same fault patch despite the relatively small coefficient of variation of their interevent times. The mechanical interpretation of this variability in seismic moment between cycles will require local datasets to determine how plate motion is accommodated differently from one cycle to the next. Does the variation in moment imply that plate motion is accommodated by a higher fraction of moderate sized events or do some regions slip seismically in one cycle and either slip aseismically (multimode behavior) or not at all in the next? In either case, owing to their high slip rates and low values of M_c, the EPR transforms will build up a dataset of mainshocks over the next ten years that will allow direct testing of particular probability distributions for the time, location, and magnitude of future large earthquakes given the history of past seismicity.

Acknowledgments

I thank Jeremy Zechar for repeatedly educating me about the intricacies of properly calculating an error diagram, and Agnes Helmstetter for providing her ETAS simulation code. I thank R. Pickle and D. Forsyth for providing their bathymetry map and plate boundary picks for the Quebrada, Discovery, and Gofar transform faults. Y. Kagan provided preprints of his work and the codes to replicate his figure of the error diagram resulting from a mixture of two renewal processes. Also, I thank Brian Atwater for discussions about quasi periodicity in subduction zones. This study utilized seismic waveform data from the IRIS-IDA, GTSN, Geoscope, IRIS-USGS, GEOFON, and NARS seismic networks archived at the IRIS datacenter. McGuire was supported by the W. M. Keck Foundation and NSF-OCE grant 0242117.

References

Behn, M. D., M. S. Boettcher, and G. Hirth (2007). On the thermal structure of oceanic transform faults, *Geology* **35,** 307–310.

Billings, S. D., M. S. Sambridge, and B. L. N. Kennett (1994). Errors in hypocenter location: picking, model, and magnitude dependence, *Bull. Seismol. Soc. Am.* **84,** 1978–1990.

Bird, P., Y. Kagan, and D. Jackson (2002). Plate tectonics and earthquake potential of spreading ridges and oceanic transform faults, in *Plate Boundary Zones*, S. Stein and J. Freymueller (Editor), AGU, Washington, D.C.

Boettcher, M., and T. H. Jordan (2004). Earthquake scaling relations for mid-ocean ridge transform faults, *J. Geophys. Res.* **109,** B12302, doi 10.1029/2004JB003110.

Bohnenstiehl, D. R., M. Tolstoy, R. P. Dziak, C. G. Fox, and D. K. Smith (2002). Aftershock sequences in the mid-ocean ridge environment: an analysis using hydroacoustic data, *Tectonophysics* **354,** 49–70.

Cisternas, M., B. Atwater, F. Torrejon, Y. Sawai, G. Machuca, M. Lagos, A. Eipert, C. Youlton, I. Salgado, T. Kamataki, M. Shishikura, C. P. Rajendran, J. K. Malik, Y. Rizal, and M. Husni (2005). Predecessors of the giant 1960 Chile earthquake, *Nature* **437,** 404–407, doi 10.1038/nature03943.

Custodio, S., and R. J. Archuleta (2007). Parkfield earthquakes: characteristic or complementary?, *J. Geophys. Res.* **112,** B05310, doi 10.1029/2006JB004617.

Dziak, R. P., C. G. Fox, R. W. Embley, J. L. Nabelek, J. Braunmiller, and R. A. Koski (2000). Recent tectonics of the Blanco Ridge, eastern Blanco transform fault zone, *Mar. Geophys. Res.* **21**, 423–450.

Ellsworth, W. L., M. V. Matthews, R. M. Nadeau, S. P. Nishenko, P. A. Reasenberg, and R. W. Simpson (1999). A physically based earthquake recurrence model for estimation of long-term earthquake probabilities, *U.S. Geol. Surv. Open-File Rept. 99-522*.

Forsyth, D. W., N. Harmon, R. C. Pickle, and A. E. Saal (2006). Stability and instability in an evolving transform fault system (Abstract T42C-01), *EOS Trans AGU* **87,** no. 52, T42C-01.

Forsyth, D. W., Y. Yang, M.-D. Mangriotis, and Y. Shen (2003). Coupled seismic slip on adjacent oceanic transform faults, *Geophys. Res. Lett.* **30,** no. 12, 1618, doi 10.1029/2002GL016454.

Fox, C. G., H. Matsumoto, and T.-K. Lau (2001). Monitoring Pacific Ocean seismicity from an autonomous hydrophone array, *J. Geophys. Res.* **106,** 4183–4206.

Global Centroid Moment Tensor (CMT) Project catalog search, www.globalcmt.org/CMTsearch.html (last accessed March 2008).

Grasso, J.-R., and I. Zaliapin (2004). Predictability of volcano eruption: lessons from a basaltic effusive volcano, *Geophys. Res. Lett.* **31,** L05602, doi 10.1029/2003GL019022.

Helmstetter, A., and D. Sornette (2002). Subcritical and supercritical regimes in epidemic models of earthquake aftershocks, *J. Geophys. Res.* **107,** 2237, doi 10.1029/2001JB001580.

Helmstetter, A., and D. Sornette (2003). Importance of direct and indirect triggered seismicity in the ETAS model of seismicity, *Geophys. Res. Lett.* **30,** no. 11, 4.

Jackson, D. D., and Y. Y. Kagan (1993). Reply: to comment of seismic gap hypothesis: ten years after, *J. Geophys. Res.* **98,** 9917–9920.

Johanson, I. A., E. J. Fielding, F. Rolandone, and R. Burgmann (2006). Coseismic and postseismic slip of the 2004 Parkfield earthquake from space-geodetic data, *Bull. Seismol. Soc. Am.* **96,** S269–S282.

Jordan, T. H. (2006). Earthquake predictability, brick by brick, *Seism. Res. Lett.* **77,** 3.

Kagan, Y. Y. (2007). On earthquake predictability measurement: information score and error diagram, *Pure Appl. Geophys.* **164,** 1947–1962.

Kagan, Y. Y., and D. D. Jackson (1991). Seismic gap hypothesis: ten years after, *J. Geophys. Res.* **96,** 21,419–21,431.

Kagan, Y., and D. D. Jackson (2000). Probabilistic forecasting of earthquakes, *J. Geophys. Res.* **86,** 438–453.

Kanamori, H., and E. E. Brodsky (2004). The physics of earthquakes, *Rep. Prog. Phys.* **67,** 1429–1496.

Kellis-Borok, V. I., P. N. Shebalin, and I. V. Zaliapin (2002). Premonitory patterns of seismicity months before a large earthquake: five case histories in southern California, *Proc. Natl. Acad. Sci. USA* **99,** 16,562–16,567.

Langmuir, C., and D. W. Forsyth (2007). Mantle melting beneath mid-ocean ridges, *Oceanography* **20,** 78–89.

Llenos, A. L., and D. W. Forsyth (2007). Apparent supershear rupture propagation on an oceanic transform fault, *Geophys. Res. Let.* (in press).

Lohman, R. B., and J. J. McGuire (2007). Earthquake swarms driven by aseismic creep in the Salton Trough, California, *J. Geophys. Res.* **112,** B04405, doi 10.1029/2006JB004596.

Lynch, J. C., R. Burgmann, M. A. Richards, and R. M. Ferencz (2003). When faults communicate: viscoelastic coupling and earthquake clustering in a simple two-fault system, *Geophys. Res. Lett.* **30,** 1270, doi 10.1029/2002GL016765.

McCann, W. R., S. P. Nishenko, L. R. Sykes, and J. Krause (1979). Seismic gaps and plate tectonics: seismic potential for major boundaries, *Pure Appl. Geophys.* **117,** 1082–1147.

McGuire, J. J., M. Boettcher, and T. H. Jordan (2005). Foreshock sequences and short-term earthquake predictability on east Pacific rise transform faults, *Nature* **434,** 457–461.

Molchan, G. M. (1997). Earthquake prediction as a decision-making problem, *Pure Appl. Geophys.*, **149,** no. 1, 233–247.

Murray, J., and P. Segall (2002). Testing time-predictable earthquake recurrence by direct measurement of strain accumulation and release, *Nature* **419,** 287–291.

Nelson, A. R., H. M. Kelsey, and R. C. Witter (2006). Great earthquakes of variable magnitude at the Cascadia subduction zone, *Quat. Res.* **65,** 354–365.

Newman, W. L., and D. L. Turcotte (2002). A simple model for the earthquake cycle combining self-organized complexity with critical point behavior, *Nonlinear Process. Geophys.* **9,** 453–461.

Nishenko, S. P., and R. Buland (1987). A generic recurrence interval distribution for earthquake forecasting, *Bull. Seismol. Soc. Am.* **77,** 1382–1399.

Nishenko, S. P., and L. R. Sykes (1993). Comment on seismic gap hypothesis: ten years after, *J. Geophys. Res.* **98,** 9909–9916.

Nishimura, C., and D. W. Forsyth (1988). Rayleigh wave phase velocities in the Pacific with implications for azimuthal anisotropy and lateral heterogeneities, *Geophys. J. R. Astr. Soc.* **94,** 479–501.

Ogata, Y. (1999). Estimating the hazard of rupture using uncertain occurrence times of paleoearthquakes, *J. Geophys. Res.* **104,** 17,995–18,014.

Reid, H. F. (1910). The mechanics of the earthquake, in *The California Earthquake of April 18, 1906, Report of the State Earthquake Investigation Commission II*, Carnegie Institute, Washington D.C.

Rice, J. (1993). Spatiotemporal complexity of slip on a fault, *J. Geophys. Res.* **98,** 9885–9907.

Roland, E., M. Boettcher, and J. J. McGuire (2004). An earthquake swarm on the Galapagos transform fault: implications for earthquake triggering (Abstract T41A-1167), *EOS Trans. AGU* **85,** no. 47 (Fall Meet. Suppl.), T41A-1167.

Searle, R. C. (1983). Multiple, closely spaced transform faults in fast-slipping fracture zones, *Geology* **11,** 607–610.

Shearer, P. M. (1997). Improving local earthquake locations using the L1 norm and waveform cross correlation: application to the Whittier Narrows, California aftershock sequence, *J. Geophys. Res.* **102,** 8269–8283.

Sykes, L. R., and W. Menke (2006). Repeat times of large earthquakes: implications for earthquake mechanics and long-term prediction, *Bull. Seismol. Soc. Am.* **96,** 1569–1596.

Sykes, L. R., B. E. Shaw, and C. H. Scholz (1999). Rethinking earthquake prediction, *Pure Appl. Geophys.* **155,** 207–232.

Trehu, A. M., and S. C. Solomon (1983). Earthquakes in the Orozco transform zone: seismicity, source mechanisms, and tectonics, *J. Geophys. Res.* **88,** 8203–8225.

Yakovlev, G., D. L. Turcotte, J. B. Rundle, and P. B. Rundle (2006). Simulation based distributions of earthquake recurrence times on the San Andreas fault system, *Bull. Seismol. Soc. Am.* **96,** 1995–2007.

Appendix

Overlapping Mainshock Pairs

Figures A1–A16 show the stations utilized, waveforms, and differential arrival times for each of the pairs from Table 2. The labels in these figures are the same as in Figure 4

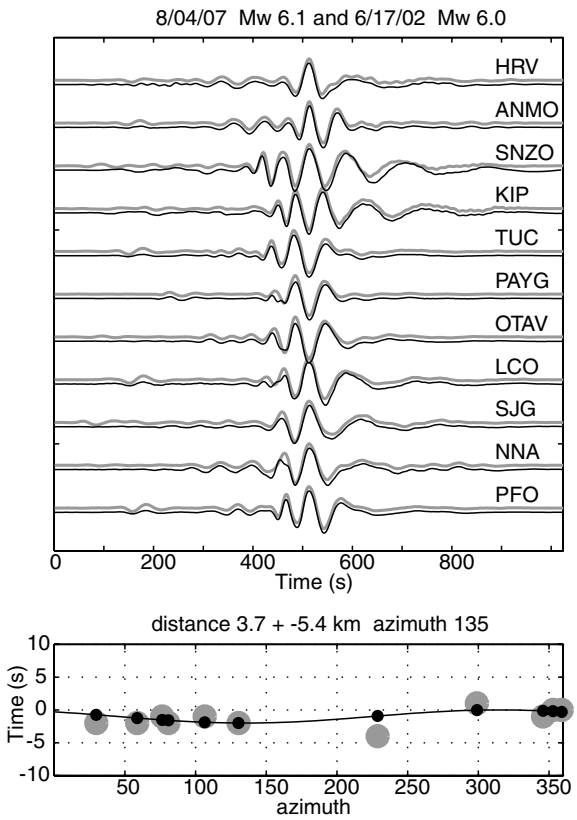

Figure A1. Event pair 1.

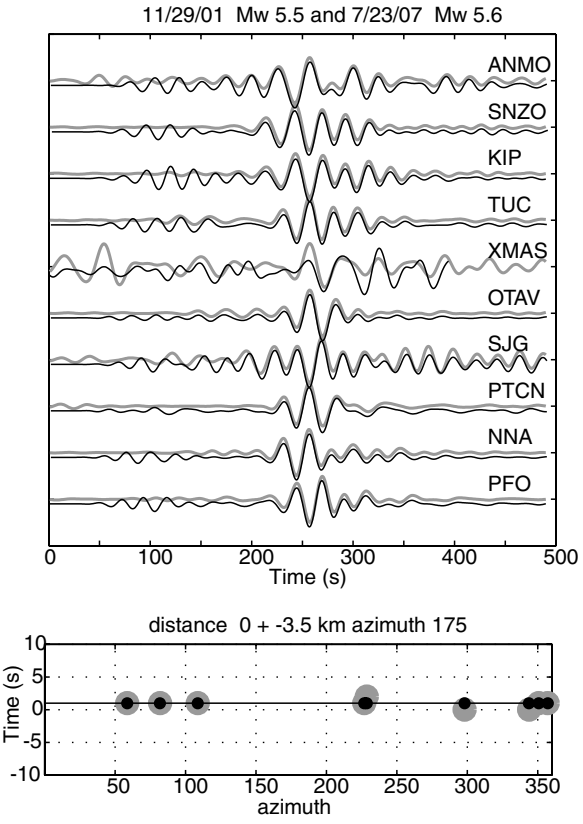

Figure A2. Event pair 2.

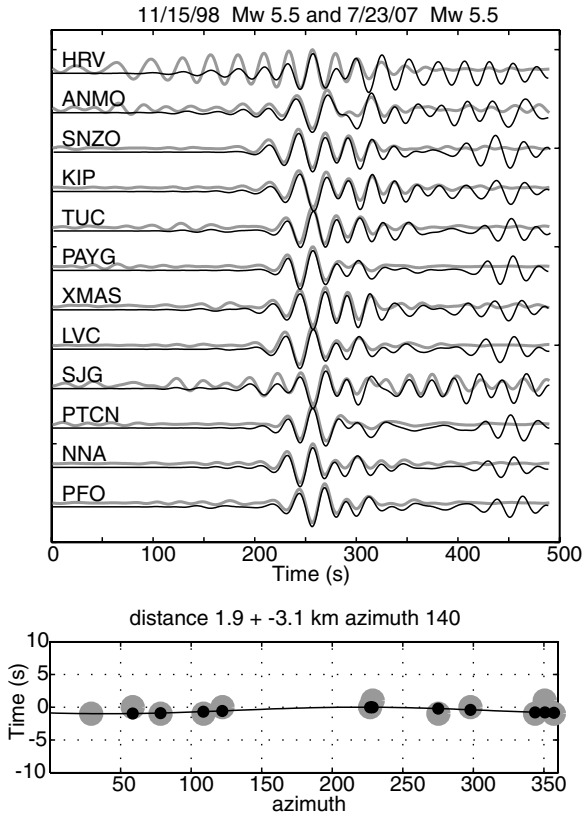

Figure A3. Event pair 3.

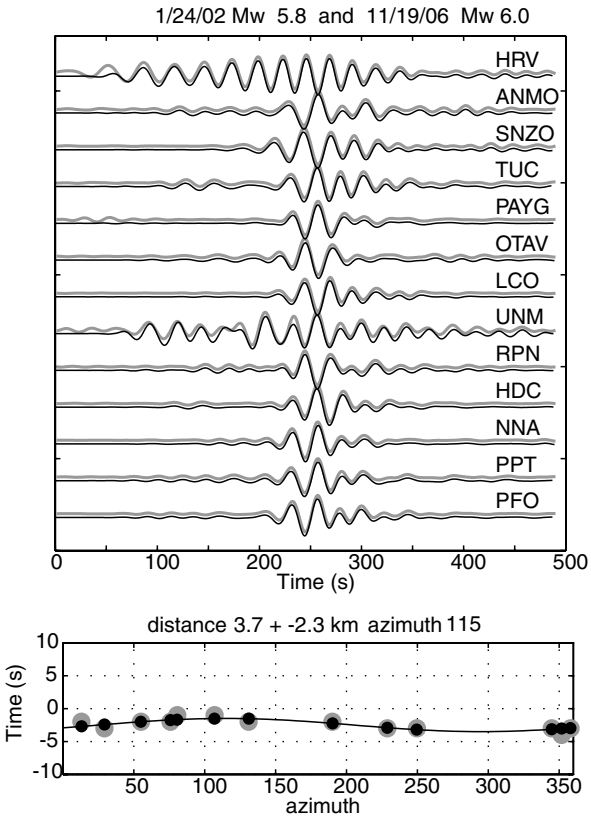

Figure A5. Event pair 5.

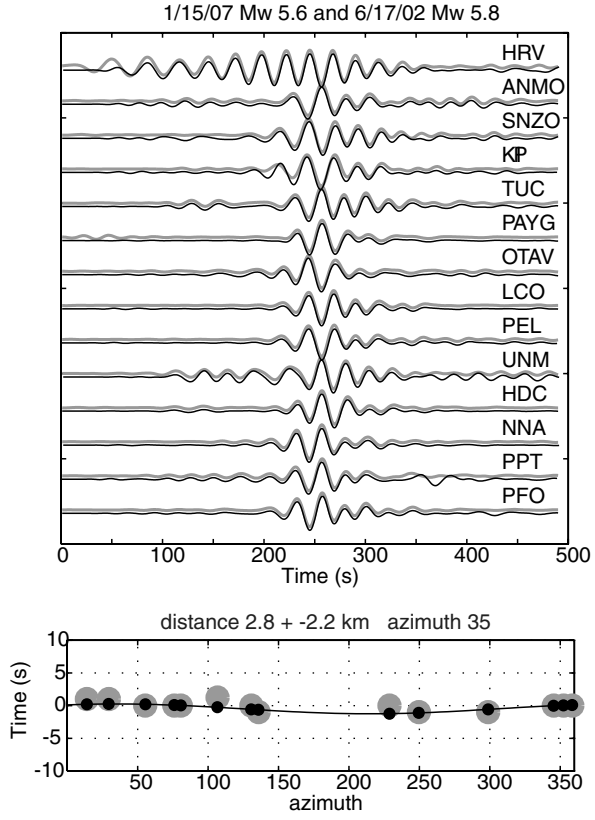

Figure A4. Event pair 4.

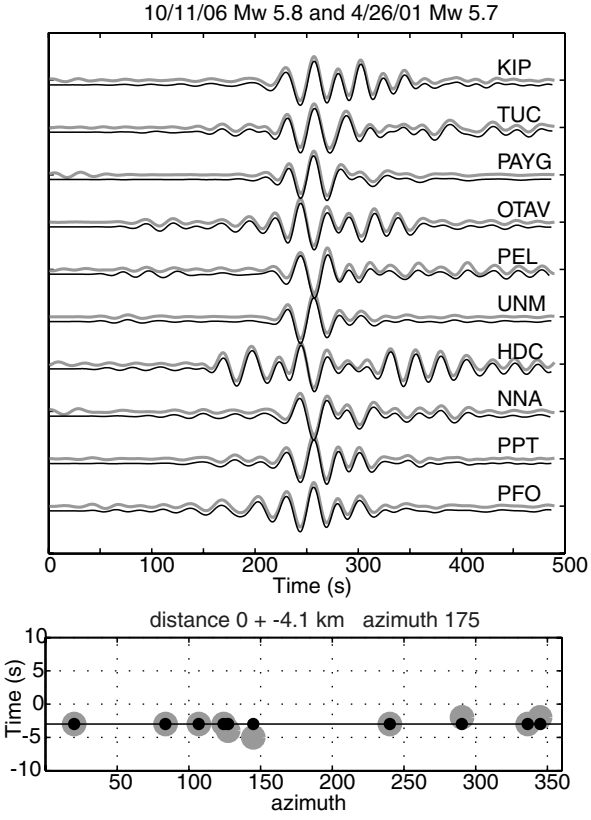

Figure A6. Event pair 6.

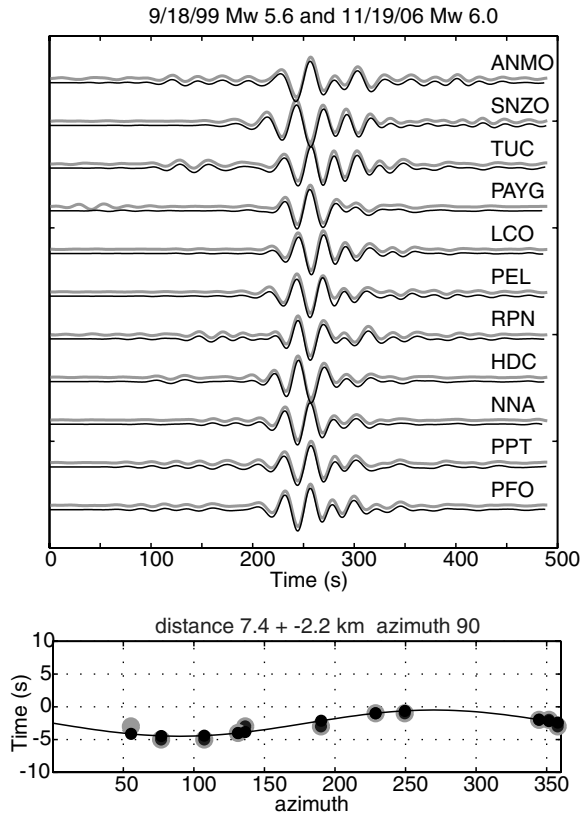

Figure A7. Event pair 7.

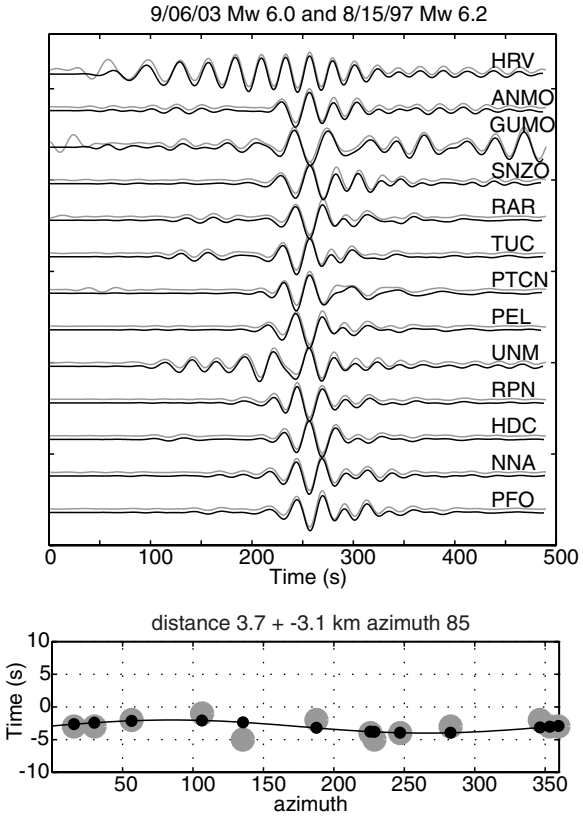

Figure A9. Event pair 9.

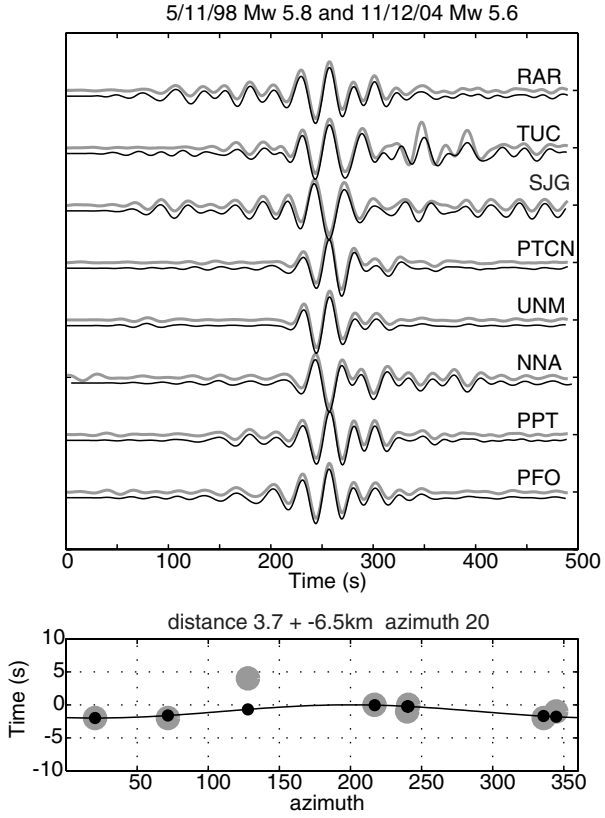

Figure A8. Event pair 8.

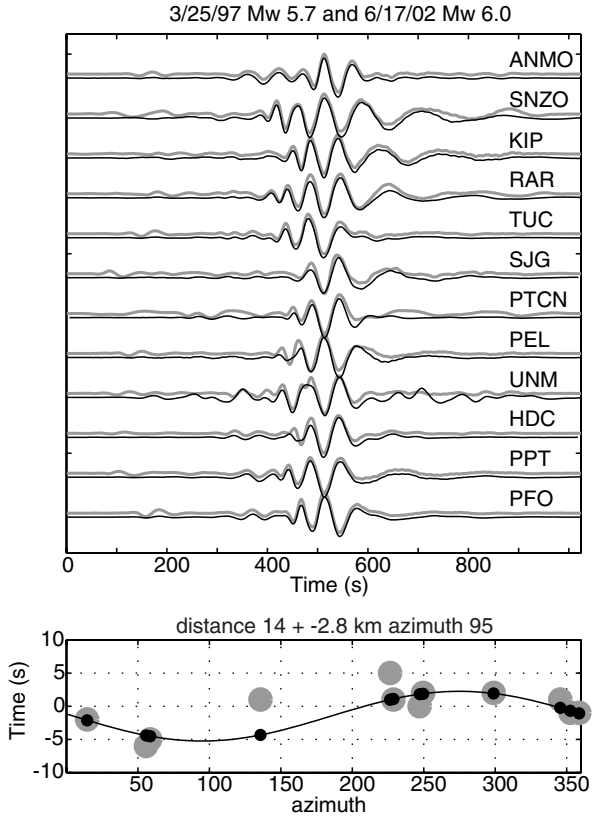

Figure A10. Event pair 10.

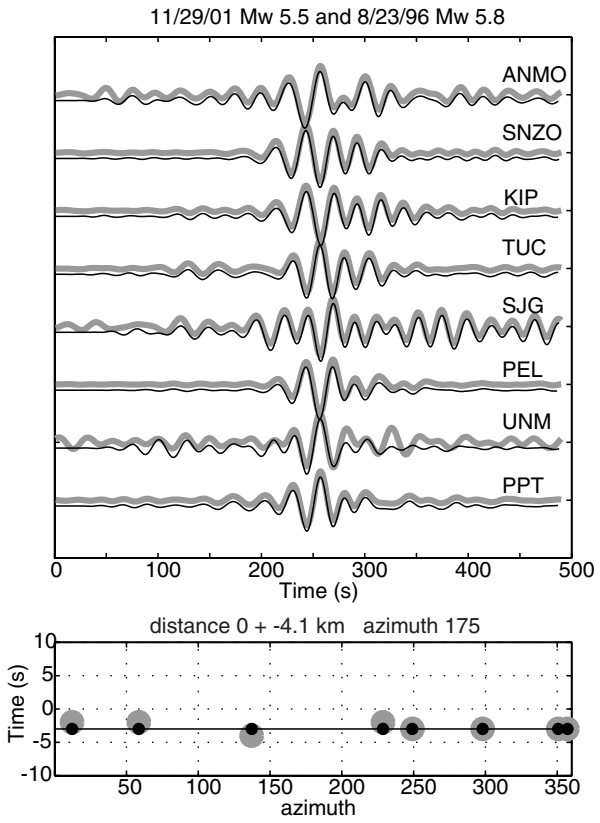

Figure A11. Event pair 11.

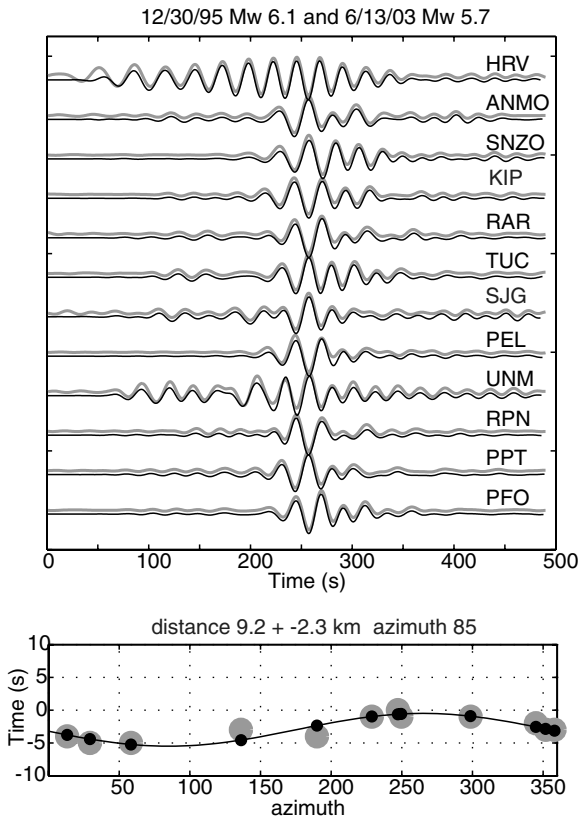

Figure A13. Event pair 13.

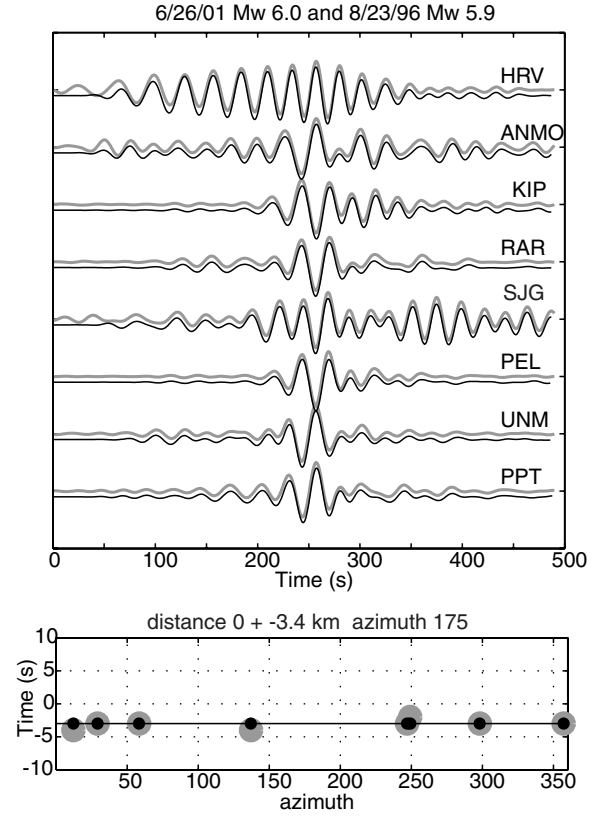

Figure A12. Event pair 12.

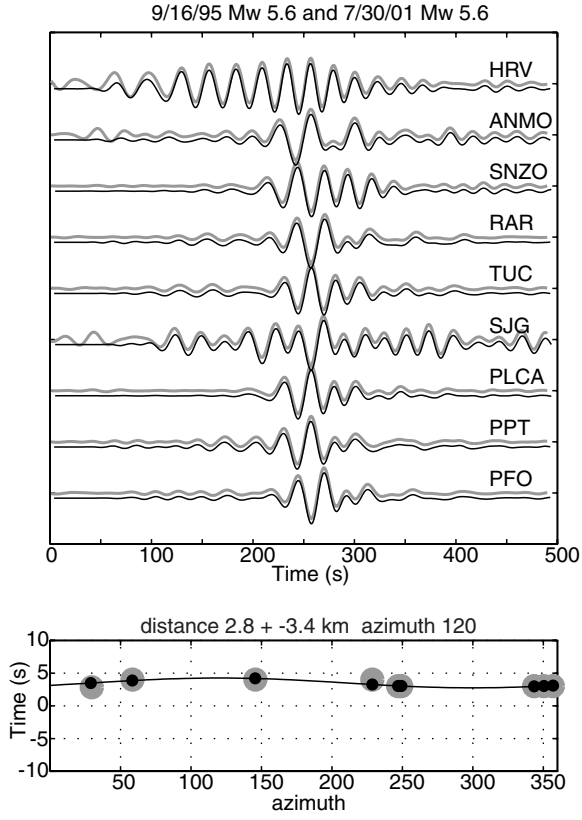

Figure A14. Event pair 14.

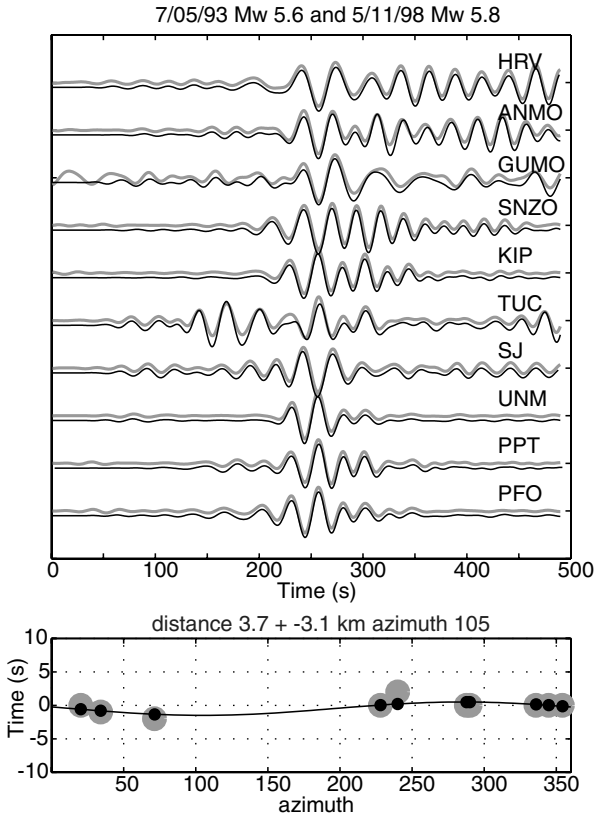

Figure A15. Event pair 15.

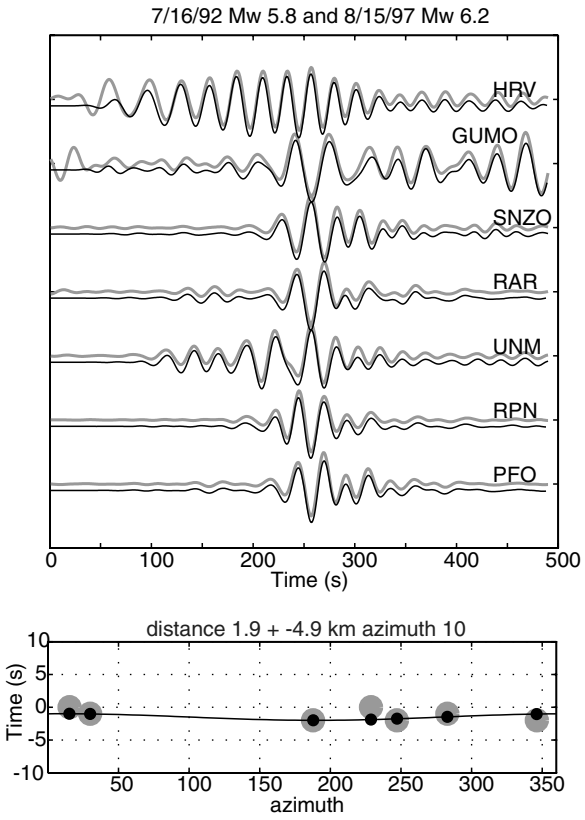

Figure A16. Event pair 16.

Department of Geology and Geophysics
Woods Hole Oceanographic Institution
Woods Hole, Massachusetts 02543
jmcguire@whoi.edu

Manuscript received 20 June 2007